

Improved positioning of surveying vessels on inland waterways with HydrOs

An article by THOMAS ARTZ, ANNETTE SCHEIDER, MARC BREITENFELD, THOMAS BRÜGGEMANN, VOLKER SCHWIEGER and HARRY WIRTH

Surveying vessels are equipped with GNSS receivers or GNSS-INS coupled systems respectively to determine their position. By receiving and processing a correction signal, which is provided by a network of continuously operating reference stations, they determine a precise GNSS real-time kinematic (GNSS-RTK) solution. Thereby, the multibeam echo sounder observations can be georeferenced in order to produce a map of the channel bottom. One crucial point of the entire workflow is the quality of the vessel position which is highly influenced by the surrounding topography. For instance, bridges or buildings can cause multipath effects, refraction or a complete loss of signal reception. Often, even the correction signals cannot be received. Then, no RTK solution can be determined. To mitigate such gaps in the GNSS-RTK trajectory, an adjustable multi-sensor system called Integrated Hydrographic Positioning System (HydrOs) was developed as a joint project of the German Federal Institute of Hydrology (Bundesanstalt für Gewässerkunde) and the Institute of Engineering Geodesy at the University of Stuttgart.

Authors

Dr. Thomas Artz is Head of the team for Hydrographic Surveying at the German Federal Institute of Hydrology (BfG).

Annette Scheider is Research Associate at the Institute of Engineering Geodesy, University of Stuttgart.

Marc Breitenfeld is Trainee for Public Service in the field of Cadastral Surveying and Mapping Authorities in Germany.

Thomas Brüggemann works in the team for Hydrographic Surveying at the German Federal Institute of Hydrology (BfG).

Prof. Dr. Volker Schwieger is Professor and Head of the Institute of Engineering Geodesy, University of Stuttgart.

Prof. Harry Wirth is Professor at the Institute of Metrology and Analysis Technique, Jade University of Applied Sciences in Oldenburg.

artz@bafg.de

GNSS | positioning | Extended Kalman Filter | hydrographic multi-sensor system | outlier testing

1 Introduction

In Germany, the Federal Waterways and Shipping Administration (Wasserstraßen- und Schifffahrtsverwaltung, WSV) has to guarantee certain water depths in waterways to ensure a smooth flow of the inland shipping and its security, i.e. basically, to allow mariners to calculate the optimal load in shallow waters. As a river's channel bottom is subject to fluctuations on time scales from days to years, the waterways have to be permanently monitored. For this purpose, echo sounding measurements are regularly performed under the patronage of the WSV. These measurements have to be georeferenced, in order to create a map or a digital terrain model of the channel. For this purpose, the absolute position of the vessel has to be known with an accuracy of at least 1 dm for the height component and 3 dm for the horizontal position, respectively.

The primary technique to determine the vessel's position at the epoch of the echo sounding measurements, and thus, to achieve the georeferencing, is the Global Navigation Satellite System (GNSS). Typically, GNSS receivers are augmented with an Inertial Measurement Unit (IMU) and a heading system to measure the orientation of the vessel in a terrestrial reference frame simultaneously. In this process, a precise Real Time Kinematic GNSS solution (GNSS-RTK) is achieved by receiving and processing a correction signal being provided by a network of continuously operating reference stations and resolving the ambiguities on-the-fly. Within the WSV, the German SAPOS Highly Precise Real-time Positioning Service (HEPS) is used. According to the SAPOS documentation (GeoBasis-DE 2015), the accuracy of this service is below 2 cm for the horizontal and 3 cm for the vertical component. Unfortunately, the solution might be significantly deteriorated

from (partial) shading due to the surrounding topography, e.g., hills, buildings, trees, or bridges. Multipath effects and loss of the correction data reception could also lead to further degradations, and, in the worst case, to a complete loss of the precise differential GNSS solution. For the purpose of monitoring inland waterways ensuring the safety of shipping traffic, this is a serious problem. Thus, the need for a more precise and most importantly more reliable positioning is obvious.

To improve the situation, i.e., to mitigate gaps in the GNSS-RTK trajectory, the Integrated Hydrographic Positioning System (HydrOs) was developed as a joint project of the department for Geodesy of the German Federal Institute of Hydrology (Bundesanstalt für Gewässerkunde, BfG) and the Institute of Engineering Geodesy (IIGS, University of Stuttgart) (Breitenfeld et al. 2014; 2015; Scheider et al. 2016). HydrOs is an integrated multi-sensor system using the entire available hardware equipment on board to determine a more reliable and robust position of the vessel. HydrOs also contains advanced models describing hydrological and vessel depending effects, e.g., a water flow model, and a squat model. For processing the measurements of the on-board sensors and the model data, an Extended Kalman Filter (EKF) (e.g., Gelb 1974) and complementary outlier tests were implemented.

2 System design

HydrOs is composed of several components, which are schematically shown in Fig. 1a. It shows the hardware components (solid boxes) which are installed on the vessel, and the models (dashed boxes). The basic core of HydrOs is the EKF with its integrity checks and outlier elimination capabilities. The output of HydrOs are coordinates, velocities and attitude information.

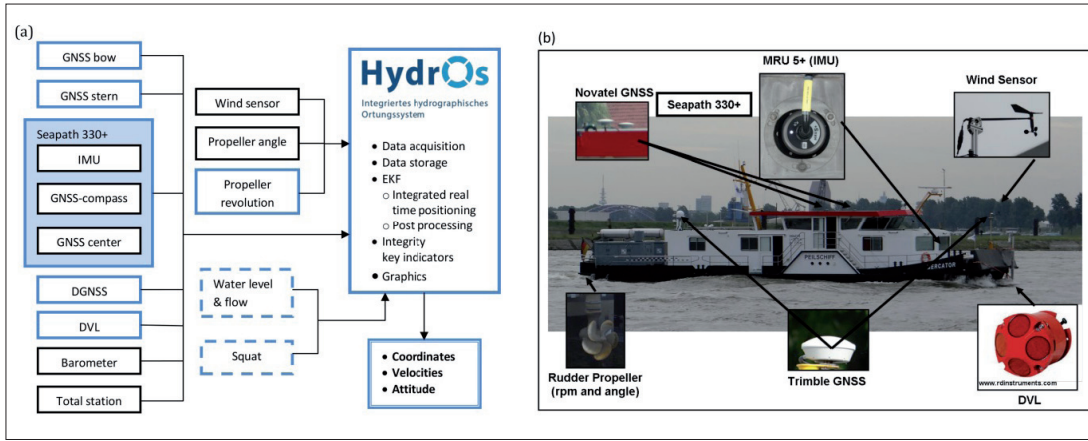


Fig. 1: (a) Sensor integration and data flow (according to Breitenfeld et al. 2014). The components which are currently adapted to the prototype are depicted in blue. The other components have just been tested. (b) Hardware components mounted to the WSV surveying vessel »Mercator« (Breitenfeld et al. 2014)

2.1 Input sensors and models

Various on-board components can be used to derive information on the motion of the vessel. For the HydrOs prototype on board of the surveying vessel »Mercator« (Fig. 1b), several GNSS receivers were used. In the test scenario, two geodetic two-frequency receivers were installed which are capable of determining a high accurate RTK solution by using SAPOS HEPS correction data. Furthermore, an integrated GNSS/INS unit (Seapath 330+) served as IMU and as GNSS compass and it also determined a RTK solution. To measure flow velocities, a Doppler Velocity Log (DVL) was appended to the measurement system. Finally, sensors were mounted to capture information about the turning rates and the direction of the two rudder propellers. However, different sensors like cameras or terrestrial laser scanners might be used in future as well. A time stamp (HydrOs reference time) is added to each incoming measurement message. The reference time is realised by synchronising the computer time with the GNSS time signal which can be extracted from the NMEA-ZDA strings according to the NMEA-0183 standard of the National Marine Electronics Association (NMEA 2016; DIN 2011). Further information on the hardware design is given by Scheider et al. (2014).

In addition to the hardware components, various models are used as input to the filtering process. The one-dimensional hydrodynamic model FLYS (FLYS 2016) is integrated to take water levels into account. Furthermore, a squat model has been derived empirically (Scheider et al. 2014) as state-of-the-art models (e.g., Briggs 2006) tend to assume too pessimistic values.

2.2 Trajectory estimation

Extended Kalman Filter

The Kalman Filter (Kalman 1960) is a linear recursive algorithm with state equations

$$x_{k+1} = T \cdot x_k + B \cdot u_k + C \cdot w_k \quad (1)$$

and measurement equations

$$l_{k+1} = A \cdot x_{k+1} + \varepsilon_{k+1} \quad (2)$$

Here, x_k represents the state vector, l_k is the measurement vector, u_k represents the system input

vector, w_k represents the process noise and ε_k the measurement noise respectively. The two noise terms are normally distributed $N(0, \Sigma_{ww})$. The matrices T , B and C describe the linear mapping of the individual variables to the following epoch. The matrix A describes the projection of the parameters into the observation space. If the prerequisites of linearity and Gaussian distribution are not fulfilled, the Kalman Filter is not the optimal estimator. To overcome the non-linearity, e.g., the Extended Kalman Filter makes use of non-linear equations ($f_{k+1,k}$, $t_{k+1,k}$, $b_{k+1,k}$, $c_{k+1,k}$ and a_{k+1}), leading to the non-linear state and measurement equations

$$x_{k+1} = f_{k+1,k}(t_{k+1,k}(x_k), b_{k+1,k}(u_k), c_{k+1,k}(w_k)) \quad (3)$$

$$l_{k+1} = a_{k+1}(x_{k+1}) + \varepsilon_{k+1} \quad (4)$$

However, the stochastic terms still have to be Gaussian. To expand the Kalman Filter to the EKF, a first-order linearisation has to be performed

$$T_{k+1,k} = \left. \frac{\partial f_{k+1,k}(t_{k+1,k}(x_k), b_{k+1,k}(u_k), c_{k+1,k}(w_k))}{\partial x_k} \right|_{x_k = \hat{x}_k} \quad (5)$$

$$B_{k+1,k} = \left. \frac{\partial f_{k+1,k}(t_{k+1,k}(x_k), b_{k+1,k}(u_k), c_{k+1,k}(w_k))}{\partial u_k} \right|_{u_k} \quad (6)$$

$$C_{k+1,k} = \left. \frac{\partial f_{k+1,k}(t_{k+1,k}(x_k), b_{k+1,k}(u_k), c_{k+1,k}(w_k))}{\partial w_k} \right|_{w_k} \quad (7)$$

$$A_{k+1} = \left. \frac{\partial a_{k+1}(x_{k+1})}{\partial x_{k+1}} \right|_{x_{k+1} = \bar{x}_{k+1}} \quad (8)$$

which leads to the linearised model

$$\bar{x}_{k+1} = T_{k+1,k} \cdot \hat{x}_k + B_{k+1,k} \cdot u_k + C_{k+1,k} \cdot w_k \quad (9)$$

$$l_{k+1} = A_{k+1} \cdot x_{k+1} + \varepsilon_{k+1} \quad (10)$$

Thus, the prediction can be calculated via the non-linear state equations

$$\bar{x}_{k+1} = f_{k+1,k}(t_{k+1,k}(\hat{x}_k), b_{k+1,k}(u_k), c_{k+1,k}(0)) \quad (11)$$

and its covariance matrix by error propagation of equation (9)

$$\Sigma_{\bar{x},k+1} = T_{k+1,k} \cdot \Sigma_{\hat{x},k} \cdot T_{k+1,k}^T + B_{k+1,k} \cdot \Sigma_{uu} \cdot B_{k+1,k}^T + C_{k+1,k} \cdot \Sigma_{ww} \cdot C_{k+1,k}^T \quad (12)$$

Subsequently, the so-called innovation and the corresponding covariance matrix

References

Breitenfeld, Marc; Harry Wirth; Annette Scheider, Volker Schwieger (2014): Development of a Multi-Sensor System to optimize the Positioning of Hydrographic Surveying Vessels; Proceedings on 4th International Conference on Machine Control & Guidance, 19–20 March 2014 in Braunschweig

Breitenfeld, Marc; Harry Wirth; Thomas Brüggemann; Annette Scheider; Volker Schwieger (2015): Entwicklung von Echtzeit- und Postprocessingverfahren zur Verbesserung der bisherigen Ortung mit Global Navigation Satellite Systems (GNSS) durch Kombination mit weiteren Sensoren sowie hydrologischen Daten; BfG-Bericht, Bundesanstalt für Gewässerkunde, <http://doi.bafg.de/BfG/2015/BfG-1856.pdf>

Briggs, Michael J. (2006): Ship Squat Predictions for Ship/Tow Simulator. Coastal and Hydraulics Engineering Technical Note CHETN-1-72; U.S. Army Engineer Research and Development Center, Vicksburg, MS

Caspary, Wilhelm; Jian-Guo Wang (1998): Redundanzanteile und Varianzkomponenten im Kalman Filter; Zeitschrift für Vermessungswesen, 123, pp. 121–128

DIN (2011): DIN 6162-1 – Navigations- und Funkkommunikationsgeräte und -systeme für die Seeschifffahrt – Digitale Schnittstellen – Teil 1: Ein Datensender und mehrere Datenempfänger; Beuth Verlag, Berlin

FLYS (2016): Flusshydrologischer Webdienst; www.bafg.de/DE/05_Wissen/01_InfoSys/flys/flys.html, last accessed on 5 July 2016

Gelb, Arthur (1974): Applied Optimal Estimation; The M.I.T. Press, Cambridge, Massachusetts

GeoBasis-DE (2015): SAPOS® Precise Positioning in Location and Height; www.sapos.de/files/SAPOS-Broschuere-2015-eng.pdf, last accessed on 5 July 2016

Kalman, Rudolph-Emil (1960): A New Approach to Linear Filtering and Prediction Problems; Transactions of the ASME-Journal of Basic Engineering, 82, pp. 35–45

Koch, Karl-Rudolf (2004): Parameterschätzung und Hypothesentests in linearen Modellen; Dümmler Verlag, Bonn

Langeley, Richard B. (1999): Dilution of Precision; GPS world, 10(5), pp. 52–59

NMEA (2016): www.nmea.org/content/nmea_standards/nmea_0183_v_410.asp, last accessed on 5 July 2016

Pelzer, Hans Georg (1987): Deformationsuntersuchungen auf der Basis kinematischer Bewegungsmodelle; Allgemeine Vermessungs-Nachrichten, 94(2), pp. 49–62 ...

$$d_{k+1} = l_{k+1} - a_{k+1} \cdot \bar{x}_{k+1} \quad (13)$$

$$\Sigma_{dd,k+1} = A_{k+1} \cdot \Sigma_{\bar{x}\bar{x},k+1} \cdot A_{k+1}^T + \Sigma_{ll} \quad (14)$$

are calculated. Finally the update

$$\hat{x}_{k+1} = \bar{x}_{k+1} + K_{k+1} \cdot d_{k+1} \quad (15)$$

$$\Sigma_{\hat{x}\hat{x},k+1} = \Sigma_{\bar{x}\bar{x},k+1} - K_{k+1} \cdot \Sigma_{dd,k+1} \cdot K_{k+1}^T \quad (16)$$

is performed via the Kalman-Gain matrix

$$K_{k+1} = \Sigma_{\bar{x}\bar{x},k+1} \cdot A_{k+1}^T \cdot \Sigma_{dd,k+1}^{-1} \quad (17)$$

Determination of redundancy values

Within the EKF solution, there is a certain amount of redundancy due to components of the state vector, the system input, the process noise, and the observations. To derive the covariance matrix of the residuals and the redundancy values, Caspary and Wang (1998) introduced pseudo observations expanded by true deviations, e.g., $\epsilon_{\hat{x},k} = \hat{x}_k - x_k$

$$l_{x,k+1} = \hat{x}_k + \epsilon_{\hat{x},k} \quad \Sigma_{\hat{x}\hat{x},k} = \Sigma_{l_x l_x, k+1} \quad (18)$$

$$l_{u,k+1} = u_k + \epsilon_{u,k} \quad \Sigma_{uu} = \Sigma_{l_u l_u, k+1} \quad (19)$$

$$l_{w,k+1} = w_k + \epsilon_{w,k} = E(w_k) \quad \Sigma_{ww} = \Sigma_{l_w l_w, k+1} \quad (20)$$

$$l_{l,k+1} = l_{k+1} = A_{k+1} \cdot \bar{x}_{k+1} + \epsilon_{l,k+1} \quad \Sigma_{ll} = \Sigma_{l_l l_l, k+1} \quad (21)$$

Based on these pseudo observations, residuals and their covariance matrices can be deduced (Wang 2009)

$$\begin{bmatrix} \hat{v}_{x,k+1} \\ \hat{v}_{u,k+1} \\ \hat{v}_{w,k+1} \\ \hat{v}_{l,k+1} \end{bmatrix} = \begin{bmatrix} \Sigma_{\hat{x}\hat{x},k} \cdot T_{k+1,k}^T \cdot \Sigma_{\bar{x}\bar{x},k+1}^{-1} \cdot K \cdot d_{k+1} \\ \Sigma_{uu} \cdot B_{k+1,k}^T \cdot \Sigma_{\bar{x}\bar{x},k+1}^{-1} \cdot K \cdot d_{k+1} \\ \Sigma_{ww} \cdot C_{k+1,k}^T \cdot \Sigma_{\bar{x}\bar{x},k+1}^{-1} \cdot K \cdot d_{k+1} \\ -\Sigma_{ll} \cdot \Sigma_{dd,k+1}^{-1} \cdot d_{k+1} \end{bmatrix} \quad (22)$$

$$\Sigma_{\hat{x}\hat{x},k+1} = \Sigma_{\hat{x}\hat{x},k} \cdot T_{k+1,k}^T \cdot A_{k+1}^T \cdot \Sigma_{dd,k+1}^{-1} \cdot A_{k+1} \cdot T_{k+1,k} \cdot \Sigma_{\hat{x}\hat{x},k} \quad (23)$$

$$\Sigma_{uu} \cdot B_{k+1,k}^T \cdot A_{k+1}^T \cdot \Sigma_{dd,k+1}^{-1} \cdot A_{k+1} \cdot B_{k+1,k} \cdot \Sigma_{uu} \quad (24)$$

$$\Sigma_{ww} \cdot C_{k+1,k}^T \cdot A_{k+1}^T \cdot \Sigma_{dd,k+1}^{-1} \cdot A_{k+1} \cdot C_{k+1,k} \cdot \Sigma_{ww} \quad (25)$$

$$\Sigma_{\hat{v}\hat{v},k+1} = (I - A_{k+1} \cdot K) \cdot \Sigma_{ll} \quad (26)$$

which are necessary to derive the redundancy values (Wang 2009)

$$r_{x,k+1} = \text{diag}\{\Sigma_{\hat{x}\hat{x},k} \cdot T_{k+1,k}^T \cdot A_{k+1}^T \cdot \Sigma_{dd,k+1}^{-1} \cdot A_{k+1} \cdot T_{k+1,k}\} \quad (27)$$

$$r_{u,k+1} = \text{diag}\{\Sigma_{uu} \cdot B_{k+1,k}^T \cdot A_{k+1}^T \cdot \Sigma_{dd,k+1}^{-1} \cdot A_{k+1} \cdot B_{k+1,k}\} \quad (28)$$

$$r_{w,k+1} = \text{diag}\{\Sigma_{ww} \cdot C_{k+1,k}^T \cdot A_{k+1}^T \cdot \Sigma_{dd,k+1}^{-1} \cdot A_{k+1} \cdot C_{k+1,k}\} \quad (29)$$

$$r_{l,k+1} = \text{diag}\{I - A_{k+1} \cdot K\} \quad (30)$$

and finally, the whole redundancy of the solution by summing up the individual redundancy values. These values are used within HydrOs to analyse the impact of any observation on the solution and to investigate its controllability.

Outlier elimination

The EKF solution can be erroneous, due to outliers or errors in the functional or stochastic modelling,

which is expressed in discrepancies between the predicted state \bar{x}_{k+1} and new observations l_{k+1} . To detect such discrepancies, the empirical variance factor

$$s_{0,j...l}^2 = \frac{\sum_{i=j}^l d_{k-i}^T \cdot \Sigma_{dd,k-i}^{-1} \cdot d_{k-i}}{\sum_{i=j}^l r_{k-i}} \quad (31)$$

is tested. It should be noted, that a local variance factor for the k th epoch is derived with $j = l = 0$. Using $l = k - 1$ leads to a global variance factor for all epochs until the most recent one, while $j < k$ yields a regional variance for $l - j + 1$ epochs. Thus, the null and alternative hypothesis read

$$H_0: E\{s_{0,k}^2\} = E\{s_{0,j...l}^2\} \quad (32)$$

$$H_A: E\{s_{0,k}^2\} \neq E\{s_{0,j...l}^2\}$$

i.e., does the local variance differ significantly from the global or regional one. Thus, the test statistics are (Pelzer 1987)

$$T = \frac{s_{0,k}^2}{s_{0,j...l}^2} = \frac{d_k^T \cdot \Sigma_{dd,k}^{-1} \cdot d_k}{r_k \cdot s_{0,j...l}^2} \sim F_{r_k, f, 1-\alpha} \quad (33)$$

f : degree of freedom in $s_{0,j...l}^2$

$r_k = n_{l,k+1}$: degree of freedom in $s_{0,k}^2$

$F_{r_k, f, 1-\alpha}$: quantile of Fisher distribution with level of significance α

A hypothesis test is performed to detect an outlier in observation i within an observation group g by using following null and alternative hypothesis (Koch 2004, p. 329)

$$H_0: v_{g,i,k} = 0 \quad (34)$$

$$H_A: v_{g,i,k} \neq 0$$

and the corresponding test statistics for a standardised residual i is

$$T = \frac{v_{g,i,k}}{\sigma_{v_{g,i,k}}} \sim N(\alpha_0, 0, 1) \quad (35)$$

α_0 : level of significance for a single observation given the entire level of significance α
 $N(\alpha_0, 0, 1)$: quantile of normal distribution

As one outlier is searched for in n observations, the level of significance has to be adapted

$$\alpha_0 \approx 1 - (1 - \alpha)^{1/n} \approx \frac{\alpha}{n \cdot (n_{\hat{x}_k} + n_{u_k} + n_{w_k} + n_{l_k})} \quad (36)$$

Finally, the null hypothesis is accepted if $-N(1 - \frac{\alpha_0}{2}, 0, 1) \leq T \leq N(1 - \frac{\alpha_0}{2}, 0, 1)$ or

$$|T| \leq N(1 - \frac{\alpha_0}{2}, 0, 1)$$

is fulfilled. As the standardised residuals can be calculated for all four groups of pseudo-observations, outliers can be detected in \hat{x}_k , u_k , w_k and l_{k+1} . The corresponding test statistics for the real observations are, e.g.,

$$T_{l_i,k+1} = \frac{\hat{v}_{l_i,k+1}}{\sigma_{\hat{v}_{l_i,k+1}}} = \frac{e_i^T \cdot \Sigma_{ll} \cdot \Sigma_{dd,k}^{-1} \cdot d_k}{\sigma_0 \cdot \sqrt{e_i^T \cdot \Sigma_{ll} \cdot \Sigma_{dd,k}^{-1} \cdot \Sigma_{ll} \cdot e_i}}$$

$$= \frac{e_i^T \cdot \Sigma_{dd,k}^{-1} \cdot d_k}{\sigma_0 \cdot \sqrt{e_i^T \cdot \Sigma_{dd,k}^{-1} \cdot e_i}} \quad (38)$$

with $i = \{1, 2, \dots, n_{l_i}\}$ (Wang 2008). Similarly, the test statistics can be derived for the other groups of pseudo observations (Breitenfeld et al. 2015). The test is performed iteratively starting with the largest standardised residual. If an outlier is detected for a (pseudo) observation, the respective observation is down-weighted, the affected matrices are recalculated and the next largest observation is tested until the null hypothesis is accepted.

Alternatively, the hypothesis test in HydrOs can be performed with studentised residuals. For this purpose, σ_0 is replaced with the empirical variance $s_{0,k}^2$ of the k th epoch. Thus, quantiles of the tau-distribution have to be used (Koch 2004, p. 332).

3 Results of the field tests

To evaluate the capability of the HydrOs system on the surveying vessel »Mercator«, several test runs were performed on the River Rhine and the channel to the port of Duisburg (Hafenkanal). The test area and the corresponding trajectories are depicted in Fig. 2. Four surveys have been performed: (1) without any shading (red), (2) with one bridge (yellow), (3) with one bridge and low vessel dynamics (green), and (4) only on parts of the red trajectory with high dynamics. Although these four surveys took place, only the results from the trajectory in the channel (green) are presented here. Furthermore, GNSS gaps have been simulated by cutting out two pieces of 62 s and 100 s, respectively. In contrast to the evaluation of real gaps, this procedure enables a comparison to the original results.

3.1 Reliability and controllability

The HydrOs solution incorporates several almost redundant measurements leading to a huge controllability of the observations. This can, e.g., be demonstrated by the redundancy values (Fig. 3) which are derived from the covariance matrix of the residuals. These numbers indicate whether a gross error shows up in the residuals of its corresponding observation or if it influences all other residuals, which can occur for small redundancy values. Thus, the redundancy values should be larger than 0.5 for a good controllability. As it can be seen in Fig. 3, the GNSS measurements are highly redundant with partial redundancies above 0.9. Therefore, filtering out individual GNSS observations does not destabilise the solution. The only observation type which is prone to undetected gross errors is the roll velocity (ω_x).

Due to the large redundancy, outliers can be easily detected. Here, a level of significance of 95 % is used as bigger problems might arise due to accepting a false null hypothesis, i.e., non-detection of outliers. Fig. 4 shows speed over ground measurements of a GNSS receiver prior to a GNSS gap. Obviously, the scatter of the time series increases

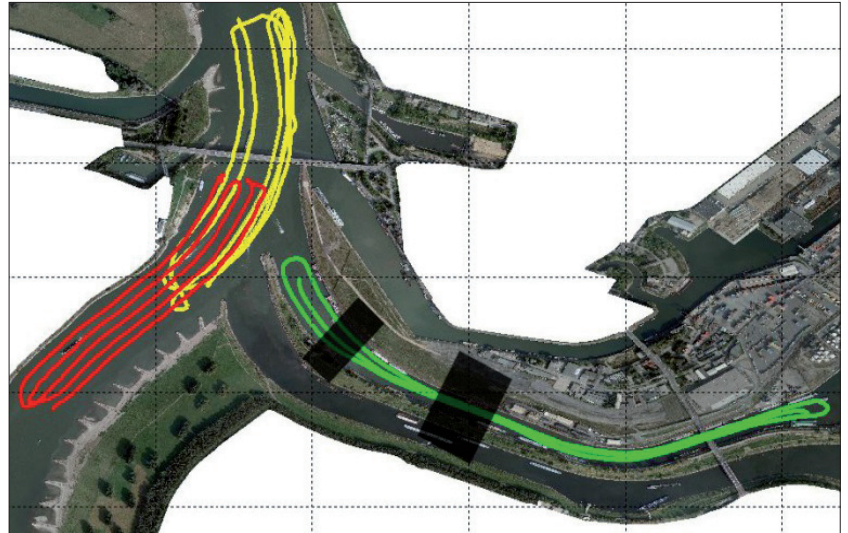


Fig. 2: Area of the test surveys with three different trajectories; the black boxes denote parts of the GNSS trajectories which have been removed to simulate large GNSS gaps (according to Wirth et al. 2015)

before the gap and observations outside the assumed noise floor are detected as outliers. Thus, the estimation is not affected by the outliers due to the huge redundancy. As in such cases, the information for the positioning is taken from other measurements.

In addition to the outlier tests within the parameter estimation, some observations can also be filtered out beforehand due to unmatched quality criteria. This has been done for the GNSS measurements, where the quality indicator (QI), number of observed satellites, and horizontal dilution of precision (HDOP) have been used. These criteria are reported by GNSS receivers. QI is a classification of the GNSS solution and easily allows excluding

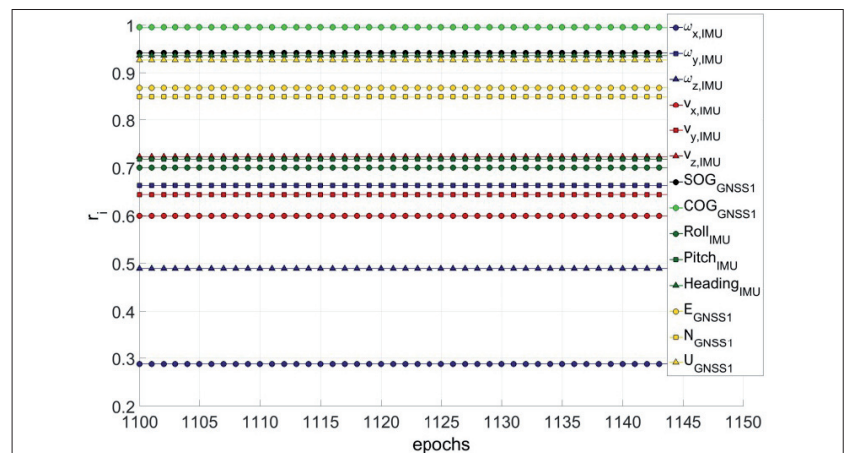


Fig. 3: Redundancy values for a subset of the different sensors, e.g., only one GNSS receiver is shown as it is representative for all of them

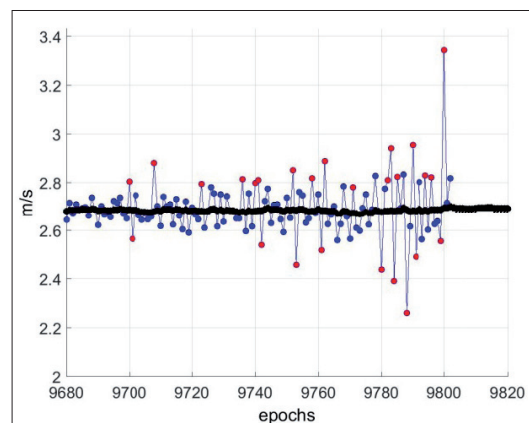


Fig. 4: Speed over ground measurements from a single GNSS receiver (blue) with marked outliers (red dots) and estimated speed over ground from the EKF solution (black)

GNSS 1	Survey 1		Survey 2		Survey 3		Survey 4	
	shading	others	shading	others	shading	others	shading	others
0–1.0 s	–	3	0	4	0	2	–	1
1.0–10.0 s	–	2	0	9	0	2	–	2
10.0 – 30.0 s	–	0	10	0	4	1	–	0
30.0–60.0 s	–	0	1	2	0	0	–	2
> 1 min	–	0	0	4	0	2	–	1
sum	–	5	11	19	4	7	–	6

positions without fixed ambiguities. DOP values permit an assumption of the quality of a GNSS solution (Langeley 1999). Applying these criteria reveals that even in unshaded areas on average 5 % to 8 % of the GNSS positions are not usable or even not recorded. A significant amount of these gaps last longer than 10 s, the absolute occurrences of gaps for one of the GNSS receiver during the four surveys are listed in the table. By utilising HydrOs, accurate positions can be determined in these regions.

3.2 Filter results

For an initial solution, the observations of one GNSS receiver and the IMU have been used. Fig. 3 shows the estimated height trajectories for this example. The EKF is not able to rectify these simulated gaps by only integrating a minimal sensor configuration, so, the trajectory is drifting away. However, the situation can be improved by adding rudder propeller revolutions as well as water-level and squat models (see Fig. 5). An assimilation of these models eliminates the drift of the EKF solution. When these EKF results are compared to the original values (without simulating the gaps), maximum deviations of about 5 cm are revealed (not shown here).

These examples demonstrate clearly the gain of using HydrOs for hydrographic surveys. Due to consistently combining the available sensors in the EKF process, a high redundancy can be achieved. Hence, outliers can be easily detected and the elimination does not harm. This way, the robustness of the solution is significantly improved. Furthermore, it has been proven that GNSS gaps of up to 60 s can be bypassed by including models into

the filtering process. The same could be achieved by implementing a backward smoother (Wirth et al. 2015).

4 Conclusions

One major issue of hydrographic measurements under the patronage of the WSV is the accuracy and reliability of the vessel's position and orientation, i.e., the GNSS-RTK solution. Within the project HydrOs, a multi-sensor system was developed which uses several on-board measurement systems (GNSS receivers and GNSS/INS system) to increase the robustness of the trajectory. In addition, hydrodynamic models and further information, i.e., a squat and a water-level model, were combined with the real measurements by means of an EKF. Especially the use of the water level model provides a reliable height solution during GNSS gaps. Furthermore, a DVL was mounted to the vessel, and the revolutions of the rudder propeller were successfully integrated.

Within the investigation, a thorough statistical analysis of the measurements is performed. As a result, it was shown that the failure rate of GNSS-RTK measurements is at the level of up to 8 %, and thus, significantly higher than expected. As a consequence, the loss of the correction signal for the RTK solution does not only lead to gaps in the trajectory, but also to position errors, which have only been determined in the past if they reached a level of several decimetres. In contrast, these discrepancies are now directly detected if HydrOs is used.

Due to the status of the project, no assessment of the net process time can be made. However, it has been demonstrated that manual corrections of the position estimates are needless when using HydrOs especially by implementing outlier detections and eliminations during the filtering process. As all the entire on-board information is used, e.g., with redundant GNSS receivers, almost all observations are well controlled which has been shown by analysing the redundancy values. The only type of measurement which is prone to undetected outliers is the angular IMU roll velocity.

Furthermore, HydrOs is providing integrity information to the users, leading to a more robust product. This is a fundamental component for warranting traffic security by WSV. [↕](#)

...
 Scheider, Annette; Harry Wirth; Marc Breitenfeld; Volker Schwieger (2014): HydrOs – An Integrated Hydrographic Positioning System for Surveying Vessels; FIG Congress 2014, 16–21 June 2014, Kuala Lumpur, Malaysia
 Scheider, Annette; Aiham Hassan; Volker Schwieger; Marc Breitenfeld; Thomas Brüggemann (2016): Erweiterte Echtzeit- und Postprocessing-Verfahren zur Optimierung der GNSS-Ortung in Abschattungsbereichen an BWaStr; BfG-Bericht, Bundesanstalt für Gewässerkunde, <http://doi.bafg.de/BfG/2016/BfG-1892.pdf>
 Wang, Jian-Guo (2008): Test Statistics in Kalman Filtering; Journal of Global Positioning Systems, 7(1), pp. 81–90
 Wang, Jian-Guo (2009): Reliability Analysis in Kalman filtering; Journal of Global Positioning Systems, 8(1), pp. 101–111
 Wirth, Harry; Marc Breitenfeld; Annette Scheider; Volker Schwieger (2015): HydrOs – Ein integriertes Ortungssystem kombiniert mit hydrologischen Daten; Hydrographische Nachrichten, HN 101, pp. 6–12

Fig. 5: Height component from GNSS-only (blue), EKF with GNSS and IMU input (grey) and EKF with GNSS, IMU and model input (black). Simulated GNSS gaps are indicated by red lines

